Journal of Physics: Conference Series **548** (2014) 012009 doi:10.1088/1742-6596/548/1/012009

Opacity profiles in inertial confinement fusion plasmas

D Benredjem[1], J C Pain[2], F Gilleron[2], S Ferri[3] and A Calisti[3]

[1] Laboratoire Aimé Cotton, Université Paris-Sud, 91405 Orsay, France
[2] CEA, DAM, DIF, F-91297 Arpajon Cedex, France
[3] Aix-Marseille Université, CNRS, PIIM, Centre Saint-Jérôme, 13397 Marseille, France

E-mail: djamel.benredjem@lac.u-psud.fr

Abstract. The opacity is an important issue in the knowledge of radiative properties of ICF and astrophysical plasmas. In this work we present the opacity of dopants embedded in the ablator of some ICF capsules. The silicon is used as dopant and we are interested in C+Si mixtures. We have used two methods to calculate the opacity of C+Si. The first one involves a detailed line shape calculation in which the atomic database is provided by a MCDF code. The lineshape code PPP is then adapted to the calculation of opacity profiles. Almost all spectral broadening effects, including Zeeman splitting and Stark effect, are taken into account. This method is able to provide accurate opacity spectra but becomes rapidly prohibitive when the number of lines is large. To account for many ionic stages and thousands of lines, a second method $-$*hybrid* method$-$ is prefered. This method combines detailed-line and statistical calculations. In the spectral regions where the lines are sufficiently separated and the number of radiative transitions is moderate, the hybrid method performs detailed calculations. When the number of transitions is very large and most of them merge in broad structures due to line broadening, the hybrid method performs statistical calculations.

1. Introduction

Indirect-drive inertial confinement fusion (ICF) uses a high-Z Hohlraum to convert precisely shaped laser pulse into thermal X-rays. The thermal radiation is absorbed due to the ablator opacity, setting up an ablation front that propagates into the ablator. Low density mass is ejected from the capsule surface, compressing the capsule in reaction (the DT fuel is compressed and a central hot spot is created at sufficiently high temperature and areal density for ignition). This spherical rocket compression process is dependent on the Hohlraum radiation temperature and on the opacity/emissivity of the ablator through the mass flux and the exhaust velocity.

The high quality of the X-ray radiation source is very important. Hard X-rays above 1.8 keV can propagate ahead of ablation front and preheat the inner layer of ablator next to the DT fuel, which increases the density difference between the fuel and ablator and results in the growth of hydrodynamic instabilities. Therefore, optimized designs of ignition capsule usually use the graded doped ablators such as germanium- or silicon-doped plastic. The role of the dopant is to absorb the hard X-ray radiation and to prevent preheating of the inner undoped plastic layer next to the DT fuel. The doped design limits Richtmyer-Meshkov and Rayleigh-Taylor instabilities as well as mixing at the fuel-ablator interface. The dopant concentration must be optimized: a too small quantity of dopant cannot efficiently prevent the preheating, and an

excess of dopant tends to reduce the implosion velocity. The knowledge of opacity is then very important.

For low- or mid-Z dopants the number of lines is sometimes tractable. In such cases, we are able to perform a detailed line calculation to obtain the opacity of silicon. This calculation involves the MCDF [1] (atomic data) and PPP [2] (line profile) codes. When the number of transitions is large this approach becomes prohibitive. An alternative approach -hybrid approach- based on a detailed description whenever it is required and a statistical one when a large number of lines overlap, is proposed. The hybrid approach for opacity is the best compromise between precision and calculation time. The statistical part is calculated by the SCO (Super-Configuration Opacity) code [3] which relies on the concept of "super-configuration".

In the next section we show results obtained by the code PPP for C+Si. In the last section we present the hybrid approach and we investigate the variation of the opacity with mass density and fraction of silicon. All ionic stages of carbon and silicon are taken into account.

2. Detailed line calculations

In a magnetized plasma, the radiators interact with a perturbing bath formed by ions in various ionic stages and free electrons. The Hamiltonian of a radiator is written as

$$H = H_0 - \mathbf{d}\cdot\mathbf{E} - \frac{\mu_B}{\hbar}(\mathbf{L}+2\mathbf{S})\cdot\mathbf{B}, \tag{1}$$

where H_0 is the Hamilonian of the free radiator. The second term in the right-hand side is the interaction of the radiator with the charged particles (free electrons and ions) that create the electric field $\mathbf{E}$. The third term represents the interaction of the magnetic moment of the radiator with the magnetic field which is due to the Rayleigh-Taylor instabilities. $\mathbf{L}$ and $\mathbf{S}$ are the orbital and spin angular momenta, respectively. μ_B is the Bohr magneton, $\mu_B = -e\hbar/(2m_e)$.

The perturbing ions are assumed static and their effect on the radiator spectrum involves a static microfield distribution function [4]. The free electrons are treated in the impact approximation and their effect on line shape is represented by a collision operator [5].

The atomic transitions occur between upper $|(\alpha)JM\rangle$ and lower $|(\alpha')J'M'\rangle$ sublevels. The polarization state is determined by the q value ($q = M - M'$). The selection rules for E1 radiation are

$$\Delta J = 0,\ \pm 1 (0 \to 0 \text{ not allowed}) \qquad q = 0,\ \pm 1.$$

Transitions with $q = \pm 1$ (0) are responsible for circularly- (linearly-) polarized radiation.

The magnetic field is assumed to be fixed along the z axis. The direction of observation forms and angle α with $\mathbf{B}$. The line profile is then given by [6]

$$I(\nu,\alpha) = I_{\parallel}\cos^2\alpha + I_{\perp}\sin^2\alpha, \tag{2}$$

where the parallel and the transverse profiles, $I_{\parallel}(\nu)$ and $I_{\perp}(\nu)$, respectively, read

$$I_{\parallel}(\nu) = I_{+}(\nu) + I_{-}(\nu), \tag{3}$$

$$I_{\perp}(\nu) = \frac{1}{4}\left[I_{+}(\nu) + I_{-}(\nu) + 2I_0(\nu)\right]. \tag{4}$$

$I_{+/-}$ (I_0) is the intensity of the right/left circularly (linearly) polarized radiation.

In the formalism of PPP, if one neglects dynamic effects the expression of each polarized line shape is written as a sum of rational fractions:

$$I_q(\nu) = \sum_p \frac{c_{q,p}(\nu-\nu_{q,p}) + a_{q,p}\gamma_{q,p}}{(\nu-\nu_{q,p})^2 + \gamma_{q,p}^2}, \tag{5}$$

where the $a_{q,p} + ic_{q,p}$ are the generalized intensities and $\nu_{q,p} + i\gamma_{q,p}$ the generalized frequencies (for more details, see Refs. [2] and [6]). Here, the line shape can be seen as the contribution of a set of Stark-Zeeman dressed transitions (SZDTs) defined by those generalized intensities and frequencies. The contribution of each SZDT to the opacity is given by:

$$k_{q,p}(\nu) = N_g \frac{\pi e^2}{mc} \frac{2m\nu_{q,p}}{3\hbar} a_{q,p} \psi_{q,p}(\nu), \tag{6}$$

where $\psi_{q,p}$ is the line shape of the SZDT and N_g the population of the ground levels. The polarized opacity is then the sum of all individual SZDTs contributions:

$$k_q(\nu) = \sum_p k_{q,p}(\nu). \tag{7}$$

In Fig. 1 we show the opacity of a mixture composed of carbon and silicon at the electron density $N_e = 6 \times 10^{23}$ cm^{-3} and temperature T_e=1000 eV. At these plasma parameter values, the fraction of non-hydrogenic ions is negligible. The gray curve accounts for electron and Doppler broadening. The black curve also accounts for the Stark effect due to perturbing ions. The comparison of the two curves shows that the ionic Stark effect is significant. In the range 250−500 eV we have carbon and silicon lines while above 600 eV we only have silicon lines.

We have checked, for several B values (from 10 MG up to 100 MG), that the Zeeman effect is negligible at these density and temperature.

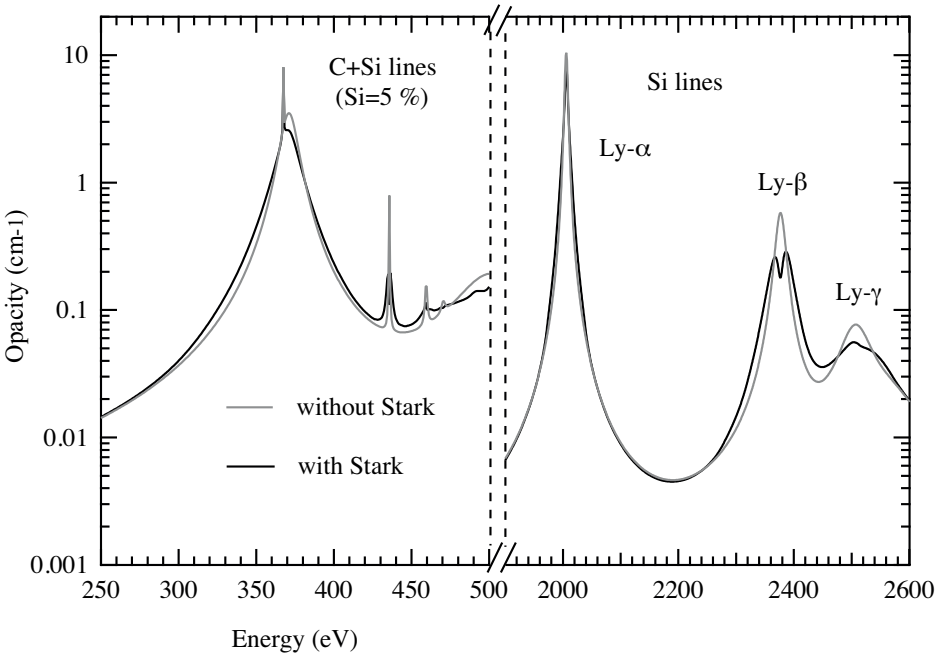

Figure 1. Opacity of the C+Si mixture. Electron density $N_e = 6 \times 10^{21}$ cm^{-3}, electron temperature T_e=1000 eV. The fraction of silicon is 5 %.

3. Hybrid calculations

Let us define some quantities which are useful in atomic spectroscopy. A non-relativistic configuration C reads $(n_1 l_1)^{N_1}(n_2 l_2)^{N_2}(n_3 l_3)^{N_3} \cdots$, where n and l are the principal and orbital

quantum numbers, respectively. N is the number of electrons occupying the sub-shell nl. The $N's$ fulfill the condition $\sum_i N_i = N_b$, where N_b is the number of bound electrons. A super-configuration (SC) reads $(\sigma_1)^{N_1}(\sigma_2)^{N_2}(\sigma_3)^{N_3}\cdots$, where the super-shell σ is an ensemble of sub-shells close in energy. Now N is the number of electrons occupying the super-shell σ. For instance $(n_1)^{N_1}(n_2)^{N_2}(n_3)^{N_3}\cdots$ is a particular case of super-configuration where all the sub-shells having the same principal quantum number are gathered. In that case, each super-shell is an ordinary shell. Note that $(n)^N$ is sometimes called a Layzer complex, but this is not true since a Layzer complex stricto sensu has a fixed parity ; therefore $(n)^N$ represents in fact two Layzer complexes. A transition array is the ensemble of transitions between two configurations of the same ion :

$$\{(n_1l_1)^{N_1}(n_2l_2)^{N_2}(n_3l_3)^{N_3}\cdots - (n_1l_1)^{N_1-1}(n_2l_2)^{N_2+1}(n_3l_3)^{N_3}\cdots\}$$

Electrons in the subshells $(n_3l_3)\cdots$ are spectators. A configuration is determined by a set of N_i: $C(N_1, N_2, N_3\cdots)$. A supertransition array (STA) [7] is the ensemble of transitions arrays $\{C(N_1, N_2, N_3\cdots) - C(N_1 - 1, N_2 + 1, N_3\cdots)\}$. The spectral broadening is often responsible for a coalescence of the lines pertaining to a transition array. In such cases the structure is named unresolved transition array (UTA) [8].

In ICF plasmas one is often faced with spectra involving a large number of lines. When most of them overlap, a detailed −line-by-line− calculation is not tractable. A statistical calculation involving the first moments of the opacity, i.e. μ_n [1], represents a satisfactory alternative. In a same spectrum we may also have separated lines which can be treated precisely, line-by-line. Then, there is a need to develop a hybrid approach which combines detailed and statistical calculations and as such would be able to treat STA and UTA structures as well as fine-structure. The hybrid code SCO-RCG [9, 10] is appropriate for such problems.

The STA approach enables one to deal with the large number of configurations but it does not provide a precise description of the individual electric-dipolar lines inside a given transition array. It can therefore be improved if several transition arrays are treated in a detailed way (line-by-line). The data required for the calculation of transition arrays (Slater integrals, spin-orbit and dipolar matrix elements) are evaluated and transmitted by SCO (Cowan's code [11] was indeed designed in such a way that the radial and dipolar integrals can be entered as parameters). Therefore, the plasma environment effects (screening) on the wave-functions are taken into account. Then, the energies of the levels and lines (positions and strengths) are calculated by an adapted RCG subroutine of Cowan's code, which performs the diagonalization of the Hamiltonian matrix (intermediate coupling).

In SCO-RCG, configuration interaction is limited to electrostatic interaction between relativistic subconfigurations (nlj orbitals) of a non-relativistic configuration (nl orbitals), namely relativistic configuration interaction (RCI). For the detailed part of the spectrum, RCI is calculated exactly, through the diagonalization of the Hamiltonian matrix. For the statistical part of the spectrum, RCI is described using an approximate model, which relies on the definition, in a transition array, of two sets of lines by considering only one relativistic orbital (the one with the largest spin-orbit integral in the transition). Corrections to the energy and strength of both structures are derived in the first-order perturbation theory, in order to include electrostatic effects between levels of the sub-arrays. Each transition array is represented by two distributions which characteristics (mean energy, strength, and number of lines) change in a continuous way from LS (where one sub-array vanishes) to jj coupling [12].

SCO-RCG involves definition of criteria in order to decide whether a detailed treatment of the lines is necessary and to determine the validity of the statistical methods. The estimate

[1] $\mu_n = \sum_{l-u} \Delta E_{lu}^n g_l f_{lu} / \sum_{l-u} g_l f_{lu}$, where ΔE_{lu}, g and f represent respectively the transition energy, the statistical weight of the lower level of the transition and the oscillator strength.

of the number of lines within a transition array is an important ingredient, in order to decide whether a detailed calculation is suitable or not for the transition array, as well as the number of levels with fixed angular momentum J which represents the size of a block of the Hamiltonian matrix. This led us to develop efficient algorithms for the numbering of LS terms and J levels [13]. We have also extended the statistical modelling of the distribution of quantum states in order to better describe configurations having open sub-shells with a large angular momentum.

Spectral broadening is taken into account. The Doppler and ionic Stark effect are modeled by a Gaussian profile. Inelastic collisions are modeled by a Lorentzian profile. The convolution of Gaussian and Lorentzian profiles yields the well-known Voigt profile. The electron collisions are described in the impact approximation within an approach proposed by Dimitrijević and Konjević [14]. Such a formulation relies on Baranger's expression for the width of an isolated line [15, 16]. The treatment of ionic Stark effect in SCO-RCG (assuming the quasi-static approximation), is very close to the one described in Refs. [17, 18]. The Zeeman line splitting is also taken into account. An approximate approach providing a fast and quite accurate estimate of the effect of an intense magnetic field on opacity was recently implemented in SCO-RCG. The formalism requires the moments of the Zeeman components of a line, which can be obtained analytically in terms of the quantum numbers and Landé factors. A good representation of the Zeeman profile is obtained using, for each component, the fourth-order Gram-Charlier expansion series [19].

In Table 1 we give for each element of the mixture, the average ion charge, the number of ionic stages involved in the hybrid calculation and the most abundant ion species.

Table 1. Average ion charge, number of ionic stages, most abundant ion. The mass density ρ and T_e are fixed to 0.01 g/cm^3 and 50 eV, respectively.

Element	$\bar{Z}$	Number of species	Most abundant ions
C	4.48	4	C^{4+}, C^{5+}
Si	8.04	8	Si^{7+}, Si^{8+}, Si^{9+}

In Fig. 2 we show the opacity of C+Si. The following spectral broadening mechanisms are included in the opacity calculation: electron impacts, ion microfield and Doppler effect. The opacity involves bound-bound, bound-free and free-free transitions. Three silicon fractions are considered: 1, 2 and 5 %. The large structure between 160 and 300 eV is composed of silicon lines. The spectral broadening due to free electrons and perturbing ions plays an important role.

Rayleigh-Taylor instabilities are expected to generate magnetic fields (see for example Ref. [20]) whose evolution depends on $\nabla N_e \times \nabla T_e$. As the magnetic field can affect the opacity, we have introduced the Zeeman effect in our opacity calculations. In Fig. 3 we compare the opacity represented in Fig. 2 and the opacity calculated with a magnetic field of 10 MG. We can see that the Zeeman effect plays a small role. A higher resolution is necessary to see the effect of the magnetic field. Then in Figure 4 we focus on a small energy interval. It is clear that the Zeeman effect plays a small role.

Figure 5 shows the variation of the opacity with density. When the density increases, the Stark broadening (electrons+ions) increases yielding a line overlapping. Moreover the number of lines decreases due to a continuum lowering. For example, the carbon peaks around 450 eV vanish at a mass density of 0.1 g/cm^3. At the highest mass density, below 150 eV the opacity is dominated by free-free transitions.

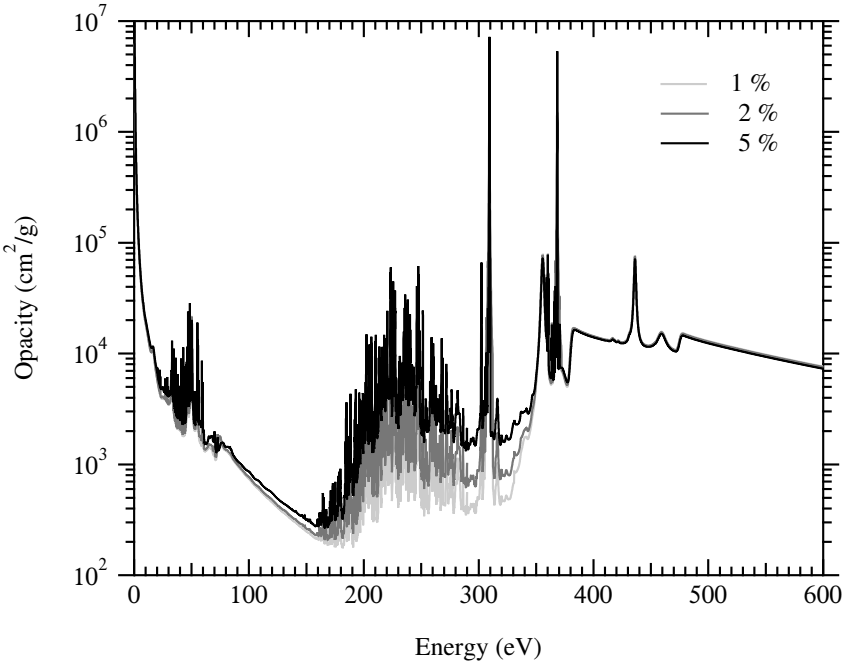

Figure 2. Opacity of C+Si for three fractions of silicon. $\rho = 0.01$ g/cm^3 and $T_e = 50$ eV.

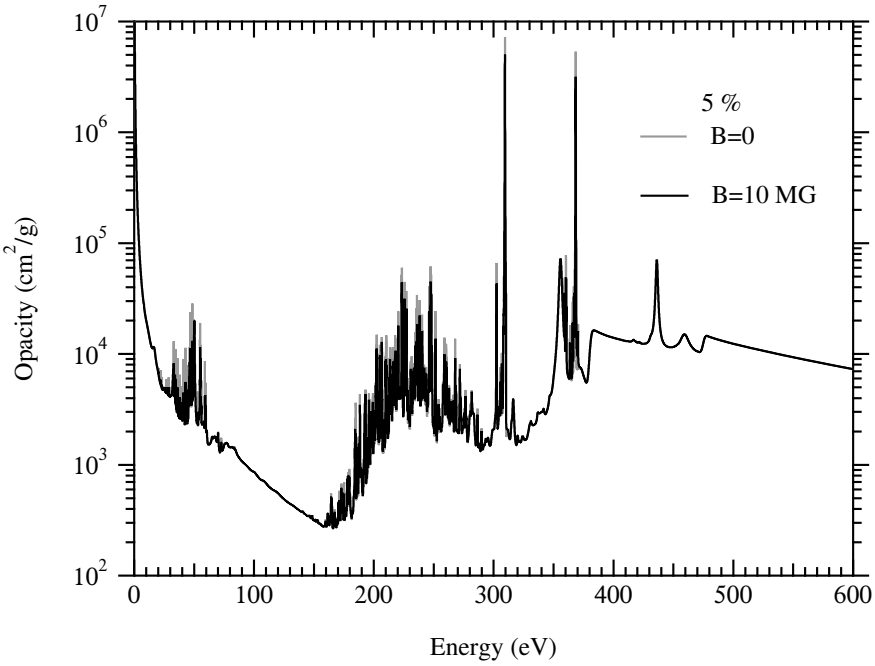

Figure 3. Opacity of C+Si. ρ and T_e, as in Fig. 2.

Finally, in Table 2 we show the variation of Rosseland and Planck mean opacities with the silicon fractions. The Planck opacity varies linearly with the silicon fraction.

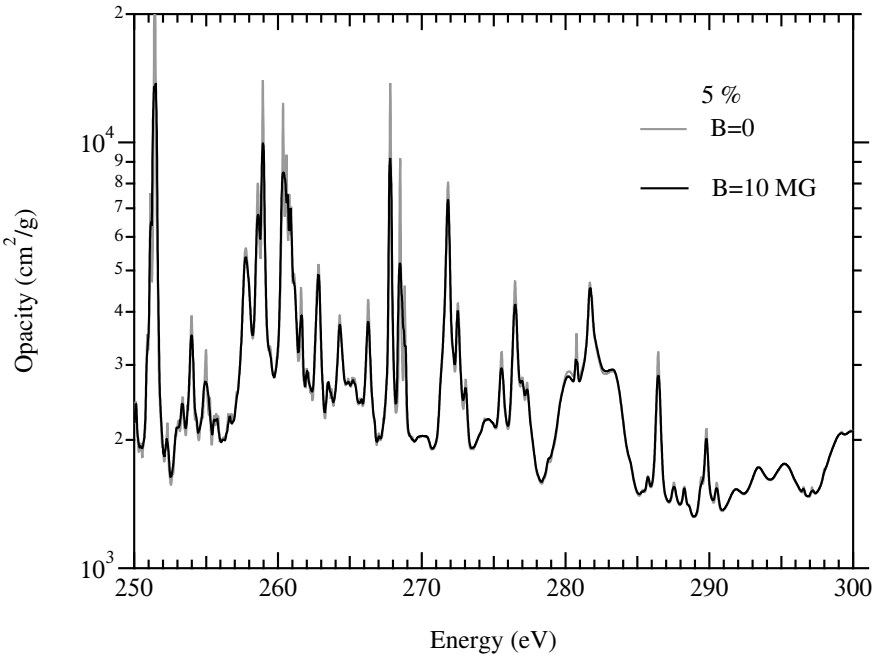

Figure 4. Same as Fig. 3 in a smaller energy interval.

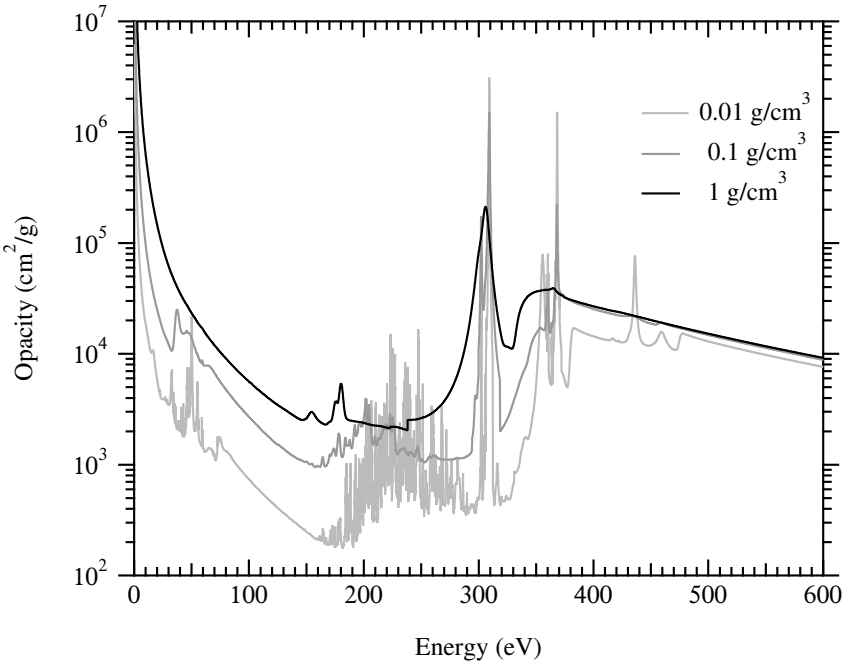

Figure 5. Opacity of C+Si for three values of ρ. T_e=50 eV and the fraction of silicon is fixed to 1%.

4. Concluding remarks

The opacity of a mixture composed of carbon and silicon is calculated for various densities and fractions of silicon. The opacity is very sensitive to both parameters. It involves a large

Table 2. Rosseland and Planck mean opacities for various silicon fractions. $\rho = 0.01$ g/cm^3 and kT_e=50 eV.

Si fraction	1%	2%	3%	4%	5%
$\kappa_{\mathrm{R}}(\times 10^2)$	5.517	7.256	8.531	9.590	10.52
$\kappa_{\mathrm{P}}(\times 10^3)$	4.949	5.196	5.437	5.671	5.900

number of lines which, owing to spectral broadening principally due to Stark effect, merge together yielding large structures. The treatment of such structures is performed with the help of statistical methods. Our calculations show that the ionic Stark effect plays an important role while the Zeeman effect is small in opacity calculations. In a future work we will investigate another dopant (Ge) and calculate the opacity of the mixture C+Ge.

References

[1] Grant I P, McKenzie B J, Norrington P H, Mayers D F and Pyper N C 1980 *Comput. Phys. Comm.* **21** 207
[2] Calisti A, Khelfaoui F, Stamm R, Talin B and Lee R W 1990 *Phys. Rev.* A **42** 5433
[3] Blenski T, Grimaldi A and Perrot F 2000 *J. Quant. Spectrosc. Radiat. Transfer* **65** 91
[4] Iglesias C A, DeWitt H E, Lebowitz J L, MacGowan D and Hubbard W B 1985 *Phys. Rev.* A **31** 1698
[5] Griem H R, Blaha M and Kepple P C 1979 *Phys. Rev.* A **19** 2421
[6] Ferri S, Calisti A, Mossé C, Mouret L and Talin B 2011 *Phys. Rev.* A **84** 026407
[7] Bar-Shalom A, Oreg J, Goldstein W H, Shvarts D and Zigler A1989 *Phys. Rev.* A **40** 3183
[8] Bauche J, Bauche-Arnoult C and Klapisch M 1979 *Phys. Rev.* A **20** 2024
[9] Porcherot Q, Pain J C, Gilleron F and Blenski T 2011 *High Energy Density Phys.* **7** 234
[10] Pain J C, Gilleron F, Porcherot Q and Blenski T 2013 *Proc. of the 40th EPS Conference on Plasma Physics* P4.403
[11] Cowan R D 1981 The Theory of Atomic Structure and Spectra, University of California Press, Berkeley
[12] Gilleron F, Bauche J and Bauche-Arnoult C 2007 *J. Phys. B: At. Mol. Opt. Phys.* **40** 3057
[13] Gilleron F and Pain J C 2009 *High Energy Density Phys.* **5** 320
[14] Dimitrijević M S and Konjević N 1987 *Astron. Astrophys.* **172** 345
[15] Baranger M 1958 *Phys. Rev.* **111** 494
[16] Baranger M 1962 in D. R. Bates, *Atomic and molecular processes* (Academic Press, New-York)
[17] Rozsnyai 1977 *J. Quant. Spectrosc. Radiat. Transfer* **17** 77
[18] Iglesias C A, Lebowitz J L and MacGowan D 1983 *Phys. Rev.* A **28** 1667
[19] Pain J C and Gilleron F 2012 *Phys. Rev.* A **85**, 033409
[20] Srinivasan B, Dimonte G and Tang X Z 2012 *Phys. Rev. Lett.* **108** 165002